



Electrical Switching of Magnetic Polarity in a Multiferroic BiFeO₃ Device at Room Temperature

N. Waterfield Price,^{1,2,*} R. D. Johnson,^{1,3} W. Saenrang,⁴ A. Bombardi,²
F. P. Chmiel,¹ C. B. Eom,⁴ and P. G. Radaelli¹

¹*Clarendon Laboratory, Department of Physics, University of Oxford,
Parks Road, Oxford OX1 3PU, United Kingdom*

²*Diamond Light Source Ltd., Harwell Science and Innovation Campus,
Didcot OX11 0DE, United Kingdom*

³*ISIS Facility, Rutherford Appleton Laboratory, Chilton, Didcot OX11 0QX, United Kingdom*

⁴*Department of Materials Science and Engineering, University of Wisconsin-Madison,
Madison, Wisconsin 53706, USA*

(Received 29 March 2017; revised manuscript received 12 June 2017; published 27 July 2017)

We have directly imaged reversible electrical switching of the cycloidal rotation direction (magnetic polarity) in a (111)_{pc}-BiFeO₃ epitaxial-film device at room temperature by nonresonant x-ray magnetic scattering. Consistent with previous reports, fully relaxed (111)_{pc}-BiFeO₃ epitaxial films consisting of a single ferroelectric domain are found to comprise a submicron-scale mosaic of magnetoelastic domains, all sharing a common direction of the magnetic polarity, which is found to switch reversibly upon reversal of the ferroelectric polarization without any measurable change of the magnetoelastic domain population. A real-space polarimetry map of our device clearly distinguishes between regions of the sample electrically addressed into the two magnetic states with a resolution of a few tens of micron. Contrary to the general belief that the magneto-electric coupling in BiFeO₃ is weak, we find that electrical switching has a dramatic effect on the magnetic structure, with the magnetic moments rotating on average by 90° at every cycle.

DOI: 10.1103/PhysRevApplied.8.014033

I. INTRODUCTION

Multiferroicity as a phenomenon is defined by the presence of an antiferromagnetic order parameter that is *quadratic* in the magnetic moments and is coupled *linearly* to the ferroelectric (FE) polarization. Different multiferroic mechanisms differ in the nature of the magnetic order parameter: for the most common cycloidal multiferroics [1], this parameter is represented by a *magnetic polarity*, and is commonly referred to as “cycloidal rotation direction” or “magnetic chirality.” For the other two known varieties—ferroaxial [2] (including *p-d* hybridized [3]) multiferroics and exchange-striction multiferroics [4]—this order parameter is represented by a magnetic helicity or a staggered exchange scalar field, respectively. Multiferroics are further classified into type I, where this order parameter is induced upon magnetic ordering in the presence of a preexisting polarization, and type II, where, conversely, the polarization is induced by the appearance of this order parameter at a magnetic transition. One important consequence of the aforementioned linear coupling is that the magnetic polarity of a cycloid can be switched through reversal of the FE polarization by an electric field. Electrical control of magnetic domains at low temperature has indeed been demonstrated on bulk single crystals of several multiferroics

by neutron polarimetry [5–7] and magnetic x-ray scattering [8]. In the latter study, Fabrizi *et al.* were able to exploit the small x-ray beam size to image the gradual switching of magnetic cycloidal domains, a technique that has since been expanded to type-I [9] and helical type-II [10] multiferroics.

Most of the multiferroic devices work carried out to date has employed the prototypical cycloidal type-I multiferroic BiFeO₃ (BFO). In this material, the direction of electric polarization can be switched within, and between, ferroelastic domains that are equivalent by pseudocubic symmetry [11]. The direction of the cycloidal propagation vector [12] and the spin-rotation plane [12–14] can also be manipulated, since they are coupled to the crystal via magnetoelastic strain [15]. In the attempt to create a prototypical memory device, these switching mechanisms have been exploited to control the magnetization of a thin ferromagnetic overlayer [16–22]. In fact, it has been shown that the overlayer magnetization can be completely reversed upon switching between 71° ferroelastic domains [19,20]—an effect that is believed to be forbidden by simple symmetry considerations. In spite of these encouraging results, there has been relatively little progress in relating macroscopic device switching to microscopic changes in the magnetic structure at the atomic level, and, in particular, to the expected reversal of the magnetic polarity. Obtaining such information in an epitaxial-film device requires a polarimetric scattering technique with

*noah.waterfieldprice@physics.ox.ac.uk

both high sensitivity and high spatial resolution—a combination that had not been achieved so far.

In this article, we present the results of a nonresonant x-ray magnetic scattering (NXMS) study in which we have directly demonstrated electrical reversal of magnetic polarity in a BFO epitaxial-film device at room temperature. In our device architecture, the full component of the electric polarization is aligned parallel to the applied (surface-normal) electric field, such that 180° switching of both electric polarization and magnetic polarity may be achieved. By combining circularly polarized x rays and postscatter polarization analysis, we determine the magnetic polarity of the cycloidal magnetic structure for two FE polarization states. We further use this to map the magnetic polarity over the device with a 50 μm \times 50 μm resolution, demonstrating that the magnetic polarity of micron-scale regions of the sample may be addressed by an electric field—an important result in the quest for practical applications of this class of materials.

The spontaneous electric polarization \mathbf{P} is directed along one of the $[111]_{\text{pc}}$ axes of the BFO pseudocubic (pc) cell and is associated with a ferroelastic distortion along the same direction, resulting in a rhombohedrally distorted perovskite structure. It has been shown that the polarization can be switched by 71°, 109°, or 180° between the eight possible $[111]_{\text{pc}}$ directions, where switching by 71°, 109° is also accompanied by a switching of the ferroelastic state [11]. Since the rhombohedral axis is unchanged when the polarization is switched by 180°, the ferroelastic domain remains unchanged. The magnetic structure of BFO can be described locally as G type but the spin-orbit interaction in the presence of the FE polarization drives an incommensurate cycloidal modulation of the spins (the direct Dzyaloshinskii-Moriya effect [23]), rotating them in a plane containing \mathbf{P} . The propagation vector of the cycloid \mathbf{k} is always orthogonal to \mathbf{P} , and can take one of three symmetry-equivalent directions in the rhombohedral lattice: $\mathbf{k}_1 = (\delta, \delta, 0)_h$, $\mathbf{k}_2 = (\delta, -2\delta, 0)_h$, $\mathbf{k}_3 = (-2\delta, \delta, 0)_h$. Here, the subscript h denotes the hexagonal setting of the rhombohedral unit cell, and $\delta = 0.0045$ at 300 K. In the case of a cycloidal magnetic structure, the quadratic order parameter is the magnetic polarity, defined as $\lambda = \mathbf{k} \times \mathbf{S}_i \times \mathbf{S}_j$, where \mathbf{S}_i and \mathbf{S}_j are spins on adjacent sites (sequential in the direction of \mathbf{k}), as depicted in Fig. 1. This appears in a term in the Landau free-energy expansion

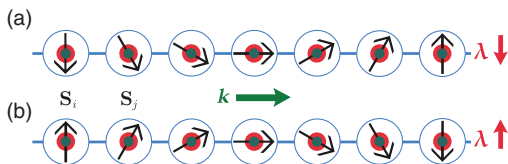


FIG. 1. Magnetic polarity. (a), (b) Magnetic spin cycloids of opposite magnetic polarity.

of the form $\propto \lambda \cdot \mathbf{P}$, which couples the FE polarization to the magnetic structure.

II. EXPERIMENTAL

1- μm -thick epitaxial films of $(111)_{\text{pc}}$ BFO are grown by double-gun off-axis sputtering onto a $(111)_{\text{pc}}$ surface-normal SrTiO_3 single-crystal substrate [24]. A 30-nm-thick SrRuO_3 layer is first deposited on the SrTiO_3 substrate by 90° off-axis sputtering before the BFO is grown, which serves as a bottom electrode [25]. 300 μm \times 200 μm \times 25 nm Pt top electrodes are patterned on the surface of the film using photolithography, which are then wirebonded to a chip carrier [see Figs. 2(a) and 2(b)]. This setup allows electric fields to be applied along the $(111)_{\text{pc}}$ direction, perpendicular to the surface of the film. As shown in Fig. 2(c), the films display excellent FE characteristics with a remnant polarization along the $[111]_{\text{pc}}$ direction of $\mathbf{P} = 102 \mu\text{C}/\text{cm}^2$, comparable to the highest reported literature values for $(111)_{\text{pc}}$ -oriented BFO films [24,26,27]. We label the FE domain with polarization directions along $[111]_{\text{pc}}$ (surface normal, pointing out of the film) and $[\bar{1}\bar{1}\bar{1}]_{\text{pc}}$ (surface normal, pointing into the film) as FE \uparrow and FE \downarrow , respectively. The as-grown state of the film is a FE \downarrow monodomain, as determined by piezoresponse force microscopy on other representative samples. Regions of the sample are switched into the FE \uparrow polarization state prior to the experiment by applying a number of successive triangular waves (see Supplemental Material [28], Part S-I) at 5 kHz, with a maximum voltage of 22 V. To test the reversibility of this process, we switch some of these regions back into the FE \downarrow polarization state, using an inverted signal.

The magnetic state of the BFO film is probed by NXMS, which can measure the direction of propagation and

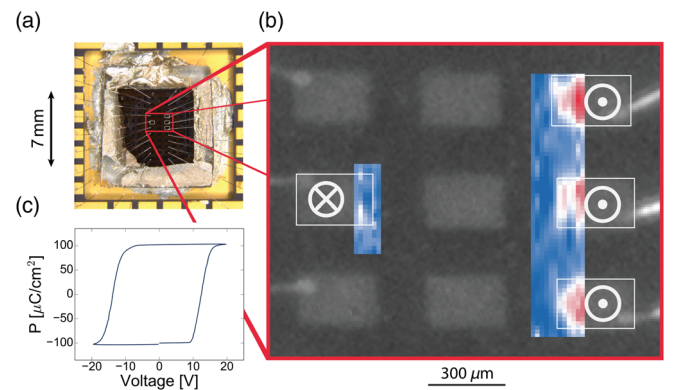


FIG. 2. $(111)_{\text{pc}}$ -BFO film device. (a) Photograph of the $(111)_{\text{pc}}$ -BFO film. (b) Optical microscope image of the $(111)_{\text{pc}}$ -BFO film surface. Maps of the magnetic polarity (see Fig. 5) are overlaid showing regions of the sample switched into the FE \downarrow and FE \uparrow state and the direction of the FE polarization is shown by the white symbols. (c) polarization–electric-field (P - E) hysteresis-loop measurement.

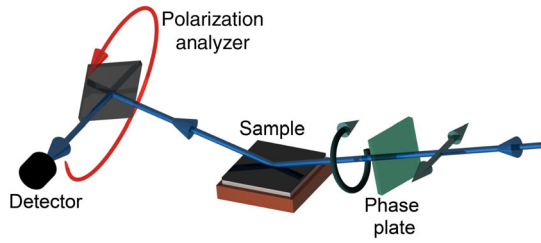


FIG. 3. Nonresonant magnetic x-ray scattering experimental setup. The incident and scattered x-ray beam directions are indicated by the blue arrows. The incident x rays are linearly polarized with their \mathbf{E} -field vector perpendicular to the scattering plane (σ polarized). These may be converted to circularly polarized x rays of either handedness using a diamond phase plate. The polarization of the scattered x rays is measured using a graphite analyzer crystal which can be rotated to select any linear polarization channel.

periodicity of the spin cycloid, as well as the spin-rotation plane. Using x-ray polarimetry, the magnetic polarity of the cycloidal magnetic structure may also be determined. The synchrotron NXMS experiments are performed on beam line I16 at Diamond Light Source (U.K.) using a six-circle kappa diffractometer in the reflection (vertical scattering) geometry, as shown in Fig. 3. The incident x-ray beam energy is tuned to 4.8 keV, which is selected for the following reasons: (a) It is off resonance of all chemical elements present in the sample. (b) Absorption both by air and the Pt electrodes on the surface of the device is minimal. (c) The probability of multiple scattering processes is reduced. Conversion of the incident x-ray polarization from σ -polarized x rays to circularly polarized x rays is achieved using a 100- μm -thick diamond quarter-wave plate. The scattered x-ray polarization is determined using a pyrolytic graphite polarization analyzer crystal scattering at the (004) reflection, built on the detector arm of the diffractometer such that any linear polarization channel may be selected. Measurements are taken at an azimuthal angle of $\phi = 94^\circ$ with respect to the $(100)_h$ direction, identified as an experimental geometry in which multiple scattering is minimized.

To determine cycloidal magnetic polarity, we measure by NXMS the magnetic satellite reflections which occur near the structurally forbidden $\mathbf{N} = (009)_h$ Bragg peak [29] using circularly polarized x rays. For a single magnetic domain with a propagation vector \mathbf{k}_i , the expected diffraction pattern is a pair of reflections located at $\mathbf{N} \pm \mathbf{k}_i$. As shown in a previous x-ray magnetic linear dichroism photoelectron emission microscopy study of an identical $(111)_{\text{pc}}$ -BFO film [29], the typical domain size is ~ 100 nm, thus approximately equal populations of all three \mathbf{k} domains fall under the x-ray spot. In this case, one would expect to observe three pairs of peaks, as depicted by the lightly shaded circles in Fig. 4(c). However, each magnetic domain is accompanied by a small monoclinic distortion, tilting the ab plane in a

direction orthogonal to \mathbf{k} . This moves the positions of the diffraction peaks such that they overlap, so that, instead of a star of six satellite peaks, only three composite peaks are observed [29] as schematically shown in Fig. 4(c).

III. RESULTS AND DISCUSSION

For a given handedness of the incident beam polarization, the diffracted signal of the magnetic satellites is sensitive to the magnetic polarity of the magnetic domains illuminated by the x-ray spot. Figures 4(a) and 4(b) show, for a region of the sample in the “virgin” $\text{FE}\downarrow$ state, reciprocal space maps of the magnetic satellites about the $\mathbf{N} = (009)_h$ position for left-circular and right-circular polarized light, respectively. Figures 4(d) and 4(e) show the equivalent measurement on a region of the sample that has been switched into the $\text{FE}\uparrow$ state. We note that, as the diffraction intensity is centered at the same point in reciprocal space for the $\text{FE}\downarrow$ and $\text{FE}\uparrow$ states, both states are in the same pseudorhombohedral ferroelastic domain. The data agree well with the corresponding simulations, shown in Figs. 4(f), 4(g) and Fig. 4(i), 4(j), respectively, and with previous measurements taken with higher statistics [29]. The simulations shown here are generated with the parameters obtained by simultaneously fitting all reciprocal space maps, with the population of the two magnetic polarity states allowed to freely refine, along with a global depolarization factor (see Supplemental Material [28], Part S-II). Here, we have assumed equal populations of the three \mathbf{k} domains, which, for this direction of the incident polarization, leads to equal intensities for the left-hand pair of peaks [labeled *A* and *B* in Fig. 4(c)]. A theoretical intensity calculation for the composite magnetic peaks shown in Fig. 4 yields

$$\frac{I_C}{I_{A,B}} \approx \frac{1 + \beta\gamma}{1 - \beta\gamma/2}, \quad (1)$$

where the subscript denotes the individual peaks, labeled as *A*, *B*, and *C* [see Fig. 4(c)] and where $\gamma = +1$ or -1 for left-circular and right-circular polarized light, respectively. The coupling between the magnetic polarity and FE polarization is parametrized by $\beta = -[(\boldsymbol{\lambda} \cdot \hat{\mathbf{n}})/|\boldsymbol{\lambda}|]$, where $\hat{\mathbf{n}}$ is the film surface normal. In agreement with a previous study on a bulk single-crystal sample [9], we find that the magnetic polarity of a given domain is aligned antiparallel to the FE polarization, hence $\beta = +1$ or -1 for the fully polarized $\text{FE}\uparrow$ state and $\text{FE}\downarrow$ state, respectively.

As shown in Figs. 4(k) and 4(l), the simultaneous fit of the reciprocal space maps yields a 93.0(6)% switch of magnetic polarity from the virgin $\text{FE}\downarrow$ state to the $\text{FE}\uparrow$ state. The depolarization factor is found to be 0.194(4) (see Supplemental Material [28], Part S-II), where this accounts for the imperfect circular polarization of the x-ray beam and contributions from any multiple scattering. The unswitched 7% could be explained by a fraction of the film being

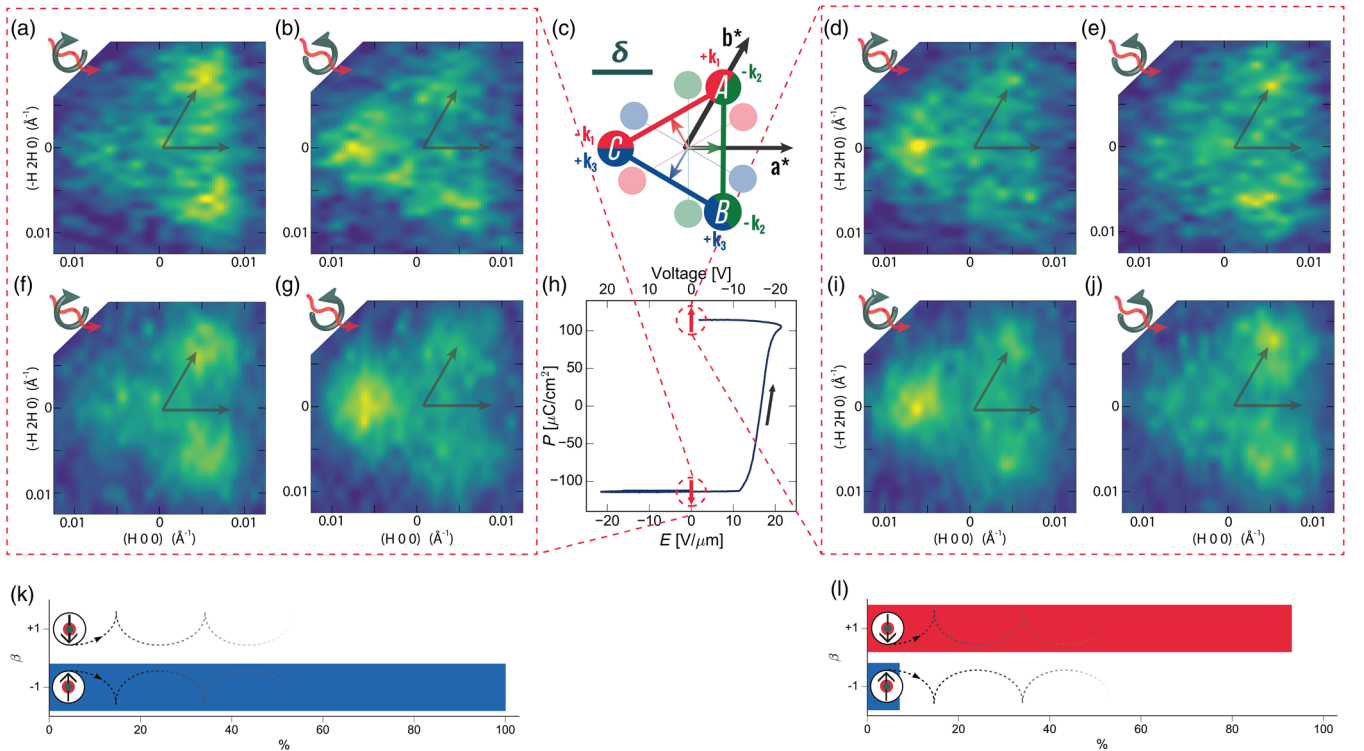


FIG. 4. Magnetic diffraction reciprocal space maps. (a), (b) NXMS reciprocal space maps about $(009)_h$ with left-circular and right-circular polarized light, respectively, in the virgin $\text{FE}\downarrow$ state. (f), (g) Fitted NXMS reciprocal space maps about $(009)_h$ with left-circular and right-circular polarized light, respectively, in the virgin $\text{FE}\downarrow$ state. (d), (e) NXMS reciprocal space maps about $(009)_h$, with left-circular and right-circular polarized light, respectively, in the switched (nominally) $\text{FE}\uparrow$ state. (i), (j) Fitted NXMS reciprocal space maps about $(009)_h$ with left-circular and right-circular polarized light, respectively, in the switched (nominally) $\text{FE}\uparrow$ state. (c) Schematic showing the effect of the monoclinic distortion on the diffracted signal, showing the undistorted (translucent) and distorted (opaque) diffraction patterns. (h) FE polarization of the sample measured while switching into the $\text{FE}\uparrow$ state. The points at which the reciprocal space maps in (a), (b) and (d), (e) are measured are labeled with \downarrow and \uparrow , respectively. The black arrow indicates the electric-field sweep direction. (k), (l) The percentage fraction of both the $\beta = +1$ and $\beta = -1$ magnetic polarities of the measured regions. The scale bar in (c) shows the magnitude of the propagation vector (all reciprocal space maps on the same scale) and the reciprocal lattice directions (in the hexagonal setting) are indicated by the translucent black arrows on the reciprocal space maps. All measurements are taken at room temperature.

pinned in the $\text{FE}\downarrow$ state, likely due to the bias at the BFO/SrRuO₃ interface that stabilizes a FE monodomain in the as-grown BFO film [31,32]. A small pinned fraction would not be detected in the FE polarization measurement in Fig. 4(h) since this measurement is relative, i.e., there is an arbitrary offset in \mathbf{P} . Furthermore, although the majority of the beam intensity is focused into an $\approx 50 \mu\text{m} \times 50 \mu\text{m}$ footprint, low intensity tails of the beam will extend slightly beyond this so it is possible that a small portion of the surrounding film in the $\text{FE}\downarrow$ state is illuminated.

The response of the magnetic structure to electrical switching is further investigated by mapping in real space the magnetic polarity over an extended region of the device. Figures 5(a) and 5(b) show real-space maps of an area of the sample containing regions that have been switched up and an area containing a region that has been switched up and then down again, respectively [see Fig. 2(c)]. These images are collected by rastering a $50 \mu\text{m} \times 50 \mu\text{m}$ beam over the sample surface and recording the intensity of peak

C at each point. The intensity is measured with both left-handed (LC) and right-handed (RC) circular polarization at every position. The maps are constructed by plotting the dichroic asymmetry $(I_{\text{LC}} - I_{\text{RC}})/(I_{\text{LC}} + I_{\text{RC}})$. In Fig. 5(a) it is clear that, for the majority of the sample region which has been switched into the $\text{FE}\uparrow$ state, the magnetic polarity has also switched relative to the unswitched film in the $\text{FE}\downarrow$ state. The areas where the magnetic polarity appears not to have switched are concentrated around the edges of the switched electrodes. This can largely be explained by the resolution limitation of the measurement [indicated by the white dotted circle in Fig. 5(a)], but it is also possible that electric-field edge effects resulted in incomplete FE switching at the outside of the pads. By contrast, the sample region below the electrical pad that has been switched into the $\text{FE}\uparrow$ state and then *back* into the $\text{FE}\downarrow$ state, has unchanged magnetic polarity relative to the surrounding region of unswitched BFO, indicating that the magnetic state is recovered entirely.

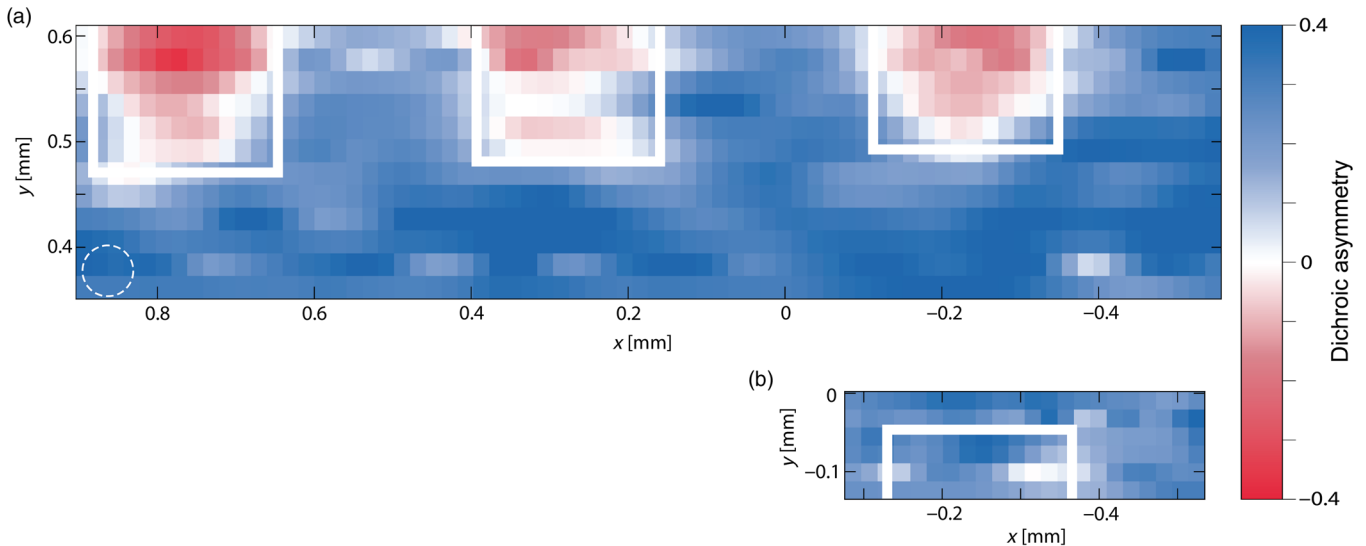


FIG. 5. Real-space maps. (a) Magnetic polarity real-space map of an area of the sample containing regions that have been switched into the $\text{FE}\uparrow$ state. The white dotted circle in the lower left corner indicates the spatial resolution of the measurement. (b) Magnetic polarity real-space map of an area of the sample containing regions that have been switched into the $\text{FE}\uparrow$ state and then switched back into the $\text{FE}\downarrow$ state. The regions underlying the Pt electrodes are outlined by the white solid lines, and the surrounding regions are in the virgin $\text{FE}\downarrow$ state. The scale and color bars refer to both (a) and (b). Based upon the characterization of switched and unswitched regions shown in Fig. 4, a dichroic asymmetry of $+0.4$ and -0.4 corresponds to a magnetic polarity of $\beta = -1$ and $\beta = +1$, respectively. x and y are two orthogonal directions that describe the lateral sample translation. These maps have been overlaid on an image of the sample in Fig. 2(c).

IV. CONCLUSION

In summary, we have demonstrated electrical switching of magnetic polarity in a BFO device at room temperature, a direct measurement of multiferroic coupling. The observed reversal of the magnetic polarity of the cycloid represents a major rearrangement of the magnetic structure, with magnetic moments rotating on average by 90° upon switching. This is in contrast to the general belief that the coupling between magnetism and ferroelectricity is rather weak in type-I multiferroics [33] but is in fact in full agreement with theoretical predictions [23]. Our experimental demonstration of polarity switching in a BFO device represents a crucial step towards developing full control of the interfacial exchange interactions in BFO-based composite multiferroic devices.

In accordance with the EPSRC policy framework on research data, access to the data is available at the link in Ref. [34].

ACKNOWLEDGMENTS

We acknowledge Diamond Light Source for time on Beam Line I16 under Proposal MT12837-1. The work done at the University of Oxford (N. W. P., R. D. J., F. P. C., and P. G. R.) is funded by EPSRC Grant No. EP/M020517/1, entitled Oxford Quantum Materials Platform Grant. The work at University of Wisconsin-Madison (C. B. E. and W. S.) is supported by the Army Research Office through Grant No. W911NF-13-1-0486. R. D. J. acknowledges support from a Royal Society University Research Fellowship.

- [1] M. Mostovoy, Ferroelectricity in Spiral Magnets, *Phys. Rev. Lett.* **96**, 067601 (2006).
- [2] R. D. Johnson, S. Nair, L. C. Chapon, A. Bombardi, C. Vecchini, D. Prabhakaran, A. T. Boothroyd, and P. G. Radaelli, $\text{Cu}_3\text{Nb}_2\text{O}_8$: A Multiferroic with Chiral Coupling to the Crystal Structure, *Phys. Rev. Lett.* **107**, 137205 (2011).
- [3] T.-h. Arima, Ferroelectricity induced by proper-screw type magnetic order, *J. Phys. Soc. Jpn.* **76**, 073702 (2007).
- [4] L. C. Chapon, G. R. Blake, M. J. Gutmann, S. Park, N. Hur, P. G. Radaelli, and S. W. Cheong, Structural Anomalies and Multiferroic Behavior in Magnetically Frustrated TbMn_2O_5 , *Phys. Rev. Lett.* **93**, 177402 (2004).
- [5] P. G. Radaelli, L. C. Chapon, A. Daoud-Aladine, C. Vecchini, P. J. Brown, T. Chatterji, S. Park, and S. W. Cheong, Electric Field Switching of Antiferromagnetic Domains in YMn_2O_5 : A Probe of the Multiferroic Mechanism, *Phys. Rev. Lett.* **101**, 067205 (2008).
- [6] Y. Yamasaki, H. Sagayama, T. Goto, M. Matsuura, K. Hirota, T. Arima, and Y. Tokura, Electric Control of Spin Helicity in a Magnetic Ferroelectric, *Phys. Rev. Lett.* **98**, 147204 (2007).
- [7] I. Cabrera, M. Kenzelmann, G. Lawes, Y. Chen, W. C. Chen, R. Erwin, T. R. Gentile, J. B. Leao, J. W. Lynn, N. Rogado, R. J. Cava, and C. Broholm, Coupled Magnetic and Ferroelectric Domains in Multiferroic $\text{Ni}_3\text{V}_2\text{O}_8$, *Phys. Rev. Lett.* **103**, 087201 (2009).
- [8] F. Fabrizi, H. C. Walker, L. Paolasini, F. de Bergevin, T. Fennell, N. Rogado, R. J. Cava, T. Wolf, M. Kenzelmann, and D. F. McMorrow, Electric Field Control of Multiferroic Domains in $\text{Ni}_3\text{V}_2\text{O}_8$ Imaged by X-ray Polarization-Enhanced Topography, *Phys. Rev. B* **82**, 024434 (2010).

- [9] R. D. Johnson, P. Barone, A. Bombardi, R. J. Bean, S. Picozzi, P. G. Radaelli, Y. S. Oh, S. W. Cheong, and L. C. Chapon, X-ray Imaging and Multiferroic Coupling of Cycloidal Magnetic Domains in Ferroelectric Monodomain BiFeO₃, *Phys. Rev. Lett.* **110**, 217206 (2013).
- [10] Y. Hiraoka, Y. Tanaka, T. Kojima, Y. Takata, M. Oura, Y. Senba, H. Ohashi, Y. Wakabayashi, S. Shin, and T. Kimura, Spin-chiral domains in Ba_{0.5}Sr_{1.5}Zn₂Fe₁₂O₂₂ observed by scanning resonant x-ray microdiffraction, *Phys. Rev. B* **84**, 064418 (2011).
- [11] F. Zavaliche, S. Y. Yang, T. Zhao, Y. H. Chu, M. P. Cruz, C. B. Eom, and R. Ramesh, Multiferroic BiFeO₃ films: Domain structure and polarization dynamics, *Phase Transitions* **79**, 991 (2006).
- [12] S. Lee, T. Choi, W. Ratcliff II, R. Erwin, S.-W. Cheong, and V. Kiryukhin, Single ferroelectric and chiral magnetic domain of single-crystalline BiFeO₃ in an electric field, *Phys. Rev. B* **78**, 100101(R) (2008).
- [13] T. Zhao, A. Scholl, F. Zavaliche, K. Lee, M. Barry, A. Doran, M. P. Cruz, Y. H. Chu, C. Ederer, N. A. Spaldin, R. R. Das, D. M. Kim, S. H. Baek, C. B. Eom, and R. Ramesh, Electrical control of antiferromagnetic domains in multiferroic BiFeO₃ films at room temperature, *Nat. Mater.* **5**, 823 (2006).
- [14] D. Lebeugle, D. Colson, A. Forget, M. Viret, A. M. Bataille, and A. Gukasov, Electric-Field-Induced Spin Flop in BiFeO₃ Single Crystals at Room Temperature, *Phys. Rev. Lett.* **100**, 227602 (2008).
- [15] D. Sando, A. Agbelele, D. Rahmedov, J. Liu, P. Rovillain, C. Toulouse, I. C. Infante, A. P. Pyatakov, S. Fusil, E. Jacquet *et al.*, Crafting the magnonic and spintronic response of BiFeO₃ films by epitaxial strain, *Nat. Mater.* **12**, 641 (2013).
- [16] Y.-H. Chu, L. W. Martin, M. B. Holcomb, M. Gajek, S.-J. Han, Q. He, N. Balke, C.-H. Yang, D. Lee, W. Hu *et al.*, Electric-field control of local ferromagnetism using a magnetoelectric multiferroic, *Nat. Mater.* **7**, 478 (2008).
- [17] H. Béa, M. Bibes, F. Ott, B. Dupé, X.-H. Zhu, S. Petit, S. Fusil, C. Deranlot, K. Bouzehouane, and A. Barthélémy, Mechanisms of Exchange Bias with Multiferroic BiFeO₃ Epitaxial Thin Films, *Phys. Rev. Lett.* **100**, 017204 (2008).
- [18] D. Lebeugle, A. Mougin, M. Viret, D. Colson, J. Allibe, H. Béa, E. Jacquet, C. Deranlot, M. Bibes, and A. Barthélémy, Exchange coupling with the multiferroic compound BiFeO₃ in antiferromagnetic multidomain films and single-domain crystals, *Phys. Rev. B* **81**, 134411 (2010).
- [19] J. T. Heron, M. Trassin, K. Ashraf, M. Gajek, Q. He, S. Y. Yang, D. E. Nikonov, Y. H. Chu, S. Salahuddin, and R. Ramesh, Electric-Field-Induced Magnetization Reversal in a Ferromagnet-Multiferroic Heterostructure, *Phys. Rev. Lett.* **107**, 217202 (2011).
- [20] J. T. Heron, J. L. Bosse, Q. He, Y. Gao, M. Trassin, L. Ye, J. D. Clarkson, C. Wang, Jian Liu, S. Salahuddin, D. C. Ralph, D. G. Schlom, J. Iniguez, B. D. Huey, and R. Ramesh, Deterministic switching of ferromagnetism at room temperature using an electric field, *Nature (London)* **516**, 370 (2014).
- [21] D. Sando, A. Barthélémy, and M. Bibes, BiFeO₃ epitaxial thin films and devices: Past, present and future, *J. Phys. Condens. Matter* **26**, 473201 (2014).
- [22] T. R. Gao, X. H. Zhang, W. Ratcliff II, S. Maruyama, M. Murakami, V. Anbusathaiah, Z. Yamani, P. J. Chen, R. Shull, R. Ramesh *et al.*, Electric-field induced reversible switching of the magnetic easy axis in Co/BiFeO₃ on SrTiO₃, *Nano Lett.* **17**, 2825 (2017).
- [23] A. M. Kadomtseva, A. K. Zvezdin, Y. F. Popov, A. P. Pyatakov, and G. P. Vorob'ev, Space-time parity violation and magnetoelectric interactions in antiferromagnets, *JETP Lett.* **79**, 571 (2004).
- [24] R. R. Das, D. M. Kim, S. H. Baek, C. B. Eom, F. Zavaliche, S. Y. Yang, R. Ramesh, Y. B. Chen, X. Q. Pan, X. Ke, M. S. Rzchowski, and S. K. Streiffer, Synthesis and ferroelectric properties of epitaxial BiFeO₃ thin films grown by sputtering, *Appl. Phys. Lett.* **88**, 242904 (2006).
- [25] C. B. Eom, R. J. Cava, R. M. Fleming, J. M. Phillips, R. B. Vandover, J. H. Marshall, J. W. Hsu, J. J. Krajewski, and W. F. Peck, Single-crystal epitaxial thin films of the isotropic metallic oxides Sr_{1-x}Ca_xRuO₃ (0 < x < 1), *Science* **258**, 1766 (1992).
- [26] J. Li, J. Wang, M. Wuttig, R. Ramesh, N. Wang, B. Ruetter, A. P. Pyatakov, A. K. Zvezdin, and D. Viehland, Dramatically enhanced polarization in (001), (101), and (111) BiFeO₃ thin films due to epitaxial-induced transitions, *Appl. Phys. Lett.* **84**, 5261 (2004).
- [27] F. Bai, J. Wang, M. Wuttig, J. Li, N. Wang, A. P. Pyatakov, A. K. Zvezdin, L. E. Cross, and D. Viehland, Destruction of spin cycloid in (111) *c*-oriented BiFeO₃ thin films by epitaxial constraint: Enhanced polarization and release of latent magnetization, *Appl. Phys. Lett.* **86**, 032511 (2005).
- [28] See Supplemental Material at <http://link.aps.org/supplemental/10.1103/PhysRevApplied.8.014033>, which includes Refs. [29,30], for further information on the preparation of the ferroelectric state of the sample and details of the nonresonant x-ray magnetic scattering data analysis.
- [29] N. Waterfield Price, R. D. Johnson, W. Saenrang, F. Maccherozzi, S. S. Dhesi, A. Bombardi, F. P. Chmiel, C. B. Eom, and P. G. Radaelli, Coherent Magnetoelastic Domains in Multiferroic BiFeO₃ Films, *Phys. Rev. Lett.* **117**, 177601 (2016).
- [30] M. Blume and D. Gibbs, Polarization dependence of magnetic x-ray scattering, *Phys. Rev. B* **37**, 1779 (1988).
- [31] D. D. Fong, A. M. Kolpak, J. A. Eastman, S. K. Streiffer, P. H. Fuoss, G. B. Stephenson, Carol Thompson, D. M. Kim, Kyoung Jin Choi, C. B. Eom *et al.*, Stabilization of Monodomain Polarization in Ultrathin PbTiO₃ Films, *Phys. Rev. Lett.* **96**, 127601 (2006).
- [32] J. E. Giencke, C. M. Folkman, S.-H. Baek, and C.-B. Eom, Tailoring the domain structure of epitaxial BiFeO₃ thin films, *Curr. Opin. Solid State Mater. Sci.* **18**, 39 (2014).
- [33] D. Khomskii, Trend: Classifying multiferroics: Mechanisms and effects, *Physics* **2**, 20 (2009).
- [34] DOI: 10.5287/bodleian:yr4XkxgGa.